# Removing upwind/downwind ambiguity of ocean wind direction by polarimetric microwave radiometer: Algorithmic basis

YIN Xiao-bin, WANG Zhen-zhan, LIU Jing-yi, JIANG Jing-shan

Center for Space Science and Applied Research, Chinese Academy of Sciences, Beijing 100190, China

Abstract: Polarimetric microwave radiometer can be used for remote sensing of ocean surface wind speed and direction. The global minimum of the cost function corresponds to the best estimate of the actual wind vector; but due to the level of noise it may not be the closest ambiguity to the true wind direction. The presence of these ambiguous solutions must be carefully considered in the retrieval of wind vector estimates. Expected errors in wind direction retrievals have been examined using Monte Carlo simulation analysis as well as the maximum likelihood estimation (MLE) cost function in the presence of noise. An algorithm is proposed to obtain wind direction according to the first and second rank solutions of the first scan and the first rank solution of the second scan. The simulated results show that the algorithm can avoid ambiguous solution, and the cells near the position that along or perpendicular to spacecraft-heading vector give the largest error of retrieved wind direction. These cells can be used for cold and warm calibration, and the residual cells which give smaller direction errors can be used for wind direction remote sensing. A new scanning geometry for conical-scan is put forward.

Key words: ocean surface wind direction; polarimetric microwave radiometer; downwind; upwind; ambiguity

CLC number: TN957.52 Document code: A

## 1 INTRODUCTION

The ocean surface wind, which generates the momentum flux affecting ocean circulation and mixing, is one of the key driving forces for the heat and moisture exchanges between the air and sea surfaces. Measurements of global wind vectors provide important information for weather forecasts and scientific studies in oceanography and climatology.

The passive microwave polarimetry is a new technology which has developed since the 1990's. Interest in using microwave radiometers for ocean wind vector measurements has increased in the past decade, because recent studies have shown that the addition of polarimetric channels can enhance wind direction retrieval performance. In January 2003, the WindSat/Coriolis mission deployed the first satellite-based fully polarimetric passive microwave instrument. The purpose of the mission is to demonstrate the capacity to obtain near-surface winds over the global oceans from passive microwave measurements (Gaiser et al, 2004). The WindSat dataset represents the first large-scale opportunity for the wind vector retrieval performance achievable by a polarimetric radiometer to be assessed. Wind vector retrievals from WindSat data have been examined in several previous studies (Bettenhausen et al, 2006; Yueh et al, 2006).

Further, the use of satellite passive microwave radiometry also has a strong heritage for remote sensing of atmospheric and oceanic environmental parameters at the same time. Wind retrievals using traditional radiometers such as AMSR (Advanced Microwave Scanning Radiometer) and SSM/I (Special Sensor Microwave/Imagers), experience a dramatic loss in accuracy in the presence of moderate and heavy rainfall and for high wind speeds. So, common wind speed algorithms of these satellites are for wind speed less than 20 m/s with no rain (Goodberlet et al, 1999; Wentz, 1992, 1997; Chang & Li, 1998). Scatterometers suffer the same problem (Weissman et al, 2003; Jones et al, 1999, 1996). With the advent of passive microwave polarimetry, an alternate tool for estimating surface wind vectors in the extreme weather conditions has become available. The performance of WindSat wind vector in Atlantic hurricanes has been evaluated by the comparison with independent surface wind field. The RMS (Root mean square) of wind direction difference is 22° where the rain rate is below 4 mm/h, while the RMS increases to 40° where the rain rate is more than 4 mm/h (Adams et al, 2006).

The objective of this study is to demonstrate methods for predicting the characteristics of errors in wind

Received date: 2007-11-05; Accepted date: 2008-05-14

First-author Biography: YIN Xiao-bin (1981— ), male. He received the Ph. D. degree in physical oceanography from the Ocean University of China, Qingdao, in 2007. His interests are in physical oceanography and ocean remote sensing, including ocean modeling, algorithm and data processing. He has published more than 20 papers.

direction retrievals and their dependence on the true wind direction relative to the observation azimuth angle. More focus is put on removing wind direction errors due to upwind/downwind ambiguous solutions. Because the assumptions regarding the combined modeling and measurement errors are simplistic, the results present here are not necessarily expected to reflect quantitatively those from actual measurements. They are instead expected to provide a useful methodology for evaluating errors encountered in real retrievals.

## 2 OVERVIEW OF WIND DIRECTION RETRIEVAL ALGORITHM AND DIRECTION AMBIGUITY

### 2.1 Principle of wind direction remote sensing

For wind-generated sea surfaces, the emission is symmetric with respect to wind direction. By building up the relationships between the four Stokes brightness temperatures and wind direction, as well as other geophysical parameters such as sea surface temperature (SST) and wind speed, we can retrieve these parameters from brightness temperatures measured by microwave polarimeter.

The brightness temperature measured by a polarimetric radiometer can be parameterized by the modified Stokes vector

$$T_B = \begin{bmatrix} T_v \\ T_h \\ T_3 \\ T_4 \end{bmatrix} = \frac{\lambda^2}{\eta k} \begin{bmatrix} \langle |E_v|^2 \rangle \\ \langle |E_h|^2 \rangle \\ 2\mathrm{Re}\langle E_v E_h^* \rangle \\ 2\mathrm{Im}\langle E_v E_h^* \rangle \end{bmatrix}, \quad (1)$$

where $E_v$ and $E_h$ are the complex amplitudes of the vertically and horizontally polarized components of the electric field in a narrow band of frequencies about a center frequency with wavelength $\lambda$. In (1), $\eta$ is the wave impedance of free space, and $k = 1.38 \times 10^{-23}$ J/K is Boltzmann's constant. The units of the Stokes vector components are in Kelvins. The Stokes parameters can be expanded in the truncated sine and cosine series (Germain et al, 2002)

$$\begin{bmatrix} T_v \\ T_h \\ T_3 \\ T_4 \end{bmatrix} = \begin{bmatrix} T_{v0} + T_{v1}\cos(\varphi) + T_{v2}\cos(2\varphi) \\ T_{h0} + T_{h1}\cos(\varphi) + T_{h2}\cos(2\varphi) \\ U_1\sin(\varphi) + U_2\sin(2\varphi) \\ V_1\sin(\varphi) + V_2\sin(2\varphi) \end{bmatrix}, \quad (2)$$

where $\varphi = \varphi_o - \varphi_w$ is the relative angle between the observation azimuth angle $\varphi_o$ and the wind direction $\varphi_w$. The first harmonics $T_{h1}$, $T_{v1}$, $U_1$ and $V_1$ account for the upwind and downwind asymmetric surface features, while the second harmonics $T_{h2}$, $T_{v2}$, $U_2$ and $V_2$ account for the upwind and crosswind asymmetry. The $\varphi_o$ in this paper is set to be $2 \times \varphi_w$, i.e. $\varphi = \varphi_w$, in order to make it simple for description and Monte Carlo analysis.

The method of maximum-likelihood estimation (MLE) was used as the basis of the wind vector retrieval algorithm (Piepmeier & Gasiewski, 2001). Under the simplifying assumption that the errors in the forward model and in the measurements are Gaussian and independent, the MLE for the wind vector is obtained by minimizing the cost function given by

$$F = \sum_{j=1}^{M} \sum_{i=1}^{N} \left( T'_{ij} - T_i \right)^2 \Delta T_{ij}^{-2}, \quad (3)$$

Here $T_{Bi}$ are the measured Stokes vector components, $u$ and $\varphi$ are the true wind speed and relative wind direction respectively, $T'_{Bi}$ are the GMF predictions for the Stokes vector components computed for a trial solution for the wind speed $u'$ and relative wind direction $\varphi'$, and N is the total number of measurement channels (frequencies and polarizations) for the system. The factors $\mathrm{Var}(T_{Bi})$ are the inverse of the combined instrument and modeling error variance estimates for each of the measurement channels. The ML retrieval problem is posed in a form allowing for the use of an arbitrary set of azimuth look angles, radiometric frequencies, and polarization states. The result is a nonlinear weighted least-squares minimization problem which can be solved using any of several multivariate search techniques.

All the wind-vector solutions found in each wind-vector cell are referred to as "ambiguities". The solutions were ranked by the magnitude of the cost function at the minimum point. The first rank solution corresponds to the global minimum of the cost function. The second rank solution corresponds to the second minimum of the cost function. Usually, 2 to 4 solutions can be derived for each wind-vector cell. The closest solution to the true wind direction is the first rank solution or the second rank solution (Piepmeier & Gasiewski, 2001).

### 2.2 Upwind/Downwind ambiguity of wind direction

Generally, the ML estimate is close to the true wind direction. Occasionally, however, a non-ML solution is significantly closer to the true wind direction, which may therefore yield a gross upwind/downwind 180° directional error (Laws et al, 2006; Liu et al, 2008).

Incorrect selection occurs because of instrument noise and geophysical modeling uncertainty, which cause the global minimum of the cost function f to occur at the incorrect direction, while one of the local minimum occurs at the correct direction. In order to characterize the structure of the local minima of the ideal cost function, the errors in wind direction associated with each cost function minimum (along with the ideal cost function magnitude at the minimum point) were recorded over a range of relative wind directions in 2° increments at 8 m/s wind speed. The results of this analysis are shown in Fig. 1. The solutions associated with this minimum appear in Fig. 1 as a horizontal line of points

with zero error. Local minima of the cost function, other than the global minimum, correspond to erroneous solutions that could be ambiguous in the presence of noises. The presence of these ambiguous solutions must be carefully considered in the retrieval of wind vector estimates and in the estimation of errors in the retrievals.

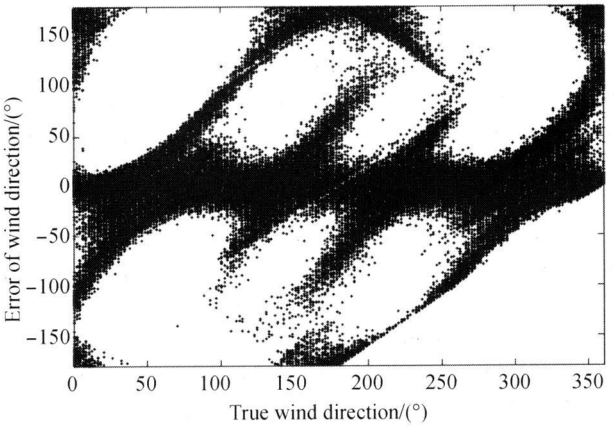


Fig. 1 Wind direction error associated with ideal cost function minima as a function of the true wind direction

The magnitude of errors observed in retrievals from simulated data carry a strong dependence on the true relative wind direction (Laws et al, 2006). In the presence of noises, the azimuth angles in the range of 0°–30° (150°–180°) could be retrieved into the range of 180°–210° (330°–360°), which rise up to 180° error of wind direction. This is caused by the wind direction harmonic character of the Stokes Vectors. Fig. 2 shows the azimuthal variation of theoretical Stokes parameters over a 360° circle at 55° incidence angle. The data were acquired using a two-scale model (Yueh, 1997) at 18.7GHz with wind speed $U_{10}$ = 8m/s at height of 10m and surface temperature $T_S$ = 290K. The upwind and downwind directions are presented as 0° and 180°, respectively. To highlight the wind direction dependence, the zeroth harmonic terms ($T_{v0}$ and $T_{h0}$) have been subtracted. As indicated by Fig. 2, the value of $T_3$ and $T_4$ is small and the sign is much alike with azimuth angle in the range of 0°–30° and 180°–200°, as well as azimuth angle in the range of 150°–180° and 330°–360°. This upwind/downwind ambiguity tends to distort the statistics so that a few such errors have a large impact on the standard deviation (Wentz et al, 2005).

To resolve the upwind/downwind ambiguity, the first harmonic of the first and second Stokes components ($T_v$ and $T_h$) should be used. However, since the relative magnitude of wind direction signal in them is two orders lower than themselves, which is almost equivalent to the instrumental noise and error of GMF for these channels, the first and second Stokes components may be of no help in removing upwind/downwind ambiguity (Laws et al, 2006).

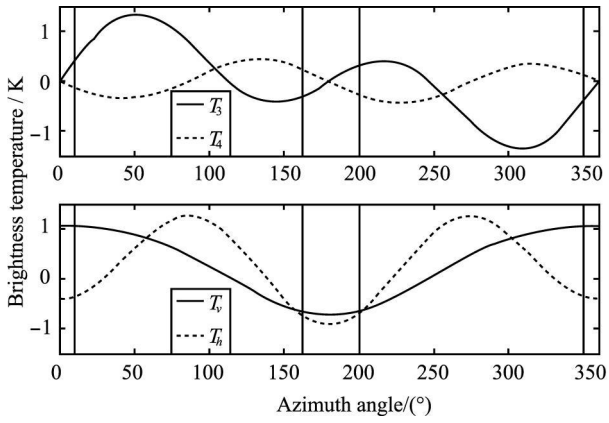


Fig. 2 Directional dependence of the four Stokes vectors with wind speed being 8m/s and surface temperature being 285K for 18.7GHz

## 3 METHOD FOR RESOLVING UPWIND/DOWNWIND AMBIGUITY

### 3.1 Monte Carlo simulation

Simulated radiometer measurements were used to investigate errors in wind vector inversions. The approach used here is based on both analysis of Monte Carlo simulations and the form of the cost function used to retrieve wind vectors.

The simulated data were generated by adding a Gaussian random component to GMF predictions of microwave brightness temperatures. The GMF we used here was based on Windrad05 Model. The empirical model Windrad05 was retuned from the empirical model Windrad99 derived from aircraft data (Yueh et al, 1999), and the retrieval analysis supported the consistency of the Windrad05 model with the Windsat data (Yueh et al, 2006). Brown (2006) also gived a model based on only Windsat data. The coefficients of $T_v$, $T_h$, $T_3$ and $T_4$ get saturated at wind speed over 15m/s in Windrad05, while only coefficients of $T_3$ and $T_4$ get saturated in Brown (2006). This difference is caused by improper atmospheric correction in Brown (2006). The coefficients given in Meissner (2002, 2005) are consistent with Windrad05. So, in this paper we used Windrad05 model as reference.

The strong response of $T_v$ and $T_h$ data to the atmospheric cloud liquid and water vapor does not allow robust wind direction estimates. In contrast, the third and fourth Stokes parameters are less sensitive to cloud and water vapor and more suitable for the ocean wind direction measurements over a broader range of weather conditions. We chose only the third and fourth Stokes parameters for analyzing wind ambiguity and developing a new algorithm to settle this problem.

Because the $T_4$ of 37Ghz in Windrad05 model is very small, the wind vector retrieval algorithm developed for the analyses used only the third and fourth stokes vectors

$T_3$ and $T_4$ of 10.7Ghz and 18.7GHz, and $T_3$ of 37Ghz. The incidence angle of each band was set to be the same as Windsat, i.e., 49.9°, 55.3°, 53° for 10.7Ghz, 18.7GHz, and 37GHz, respectively. Then, the cost function would be (Yueh et al, 2006)

$$f=\sum_{i=1}^{3}\frac{[T_{3,4i}(u,\varphi)-T_{3,4i}(u',\varphi')]^2}{\mathrm{Var}(T_{3,4i})} \quad (4)$$

A measurement noise standard deviation of 0.4 K was assumed for all $T_3$ channels, 0.25 K for all $T_4$ channels, and standard deviation of 2m/s for retrieved wind speed. Here, the measurement noise is a root-sum-squared combination of both instrument noise and GMF (errors of model atmospheric parameters and SST) errors. The process of generating simulated data with random errors and inverting to obtain wind vector estimates was repeated 625 times (25×25 grid) for each wind direction, over the full range of wind directions in 2° increment. Under the assumption of Gaussian independent errors, it obtained solutions for the wind vector by minimizing the cost function (4). A combination of grid search and minimum locating techniques was employed to ensure that all minima of the cost function were precisely located.

Due to regression errors, the first rank (most likely) solution is not always the closest ambiguity to the true wind direction. We applied a spatial vector median filter (MF) to the retrieval cells to correct isolated errors in the ambiguity selection based on MLE. The MF is an iterative spatial filter that selects from the set of ambiguities in the cell being filtered the one most consistent with the previously selected ambiguities in a window of surrounding cells. It accomplishes this by minimizing the vector median filter function, a weighted sum of norms of vector differences between an ambiguity and the previously selected ambiguities for all cells in the window.

In our application, the window was set to 7×7 cells (in scan-based coordinates) centered on and including the cell being filtered (Smith et al, 2006; Shaffer et al, 1991). The MF was initialized with the first rank wind vector from each ocean retrieval cell. If a retrieved wind direction was more than 20° different from the median filter output, the next most likely direction would be tested for a better fit. The next most likely direction was chosen if it fell within the 20° window, otherwise the original ML estimate was retained (Piepmeier and Gasiewski, 2001). After the MF was applied to all ocean cells in an orbit, the newly selected wind field replaced the previous wind field. The process was iterated until the wind field converges.

### 3.2 Algorithm for resolving upwind/downwind ambiguity

If there are two measurements in different scan angles, the third and fourth Stokes vector components being zero along the upwind and downwind directions in one scan will become nonzero in the other. Thus wind direction ambiguities can be isolated using the third and fourth Stokes vector of the second scan, as indicated in Fig. 3. The difference of scan angle in Fig. 3 is 80°.

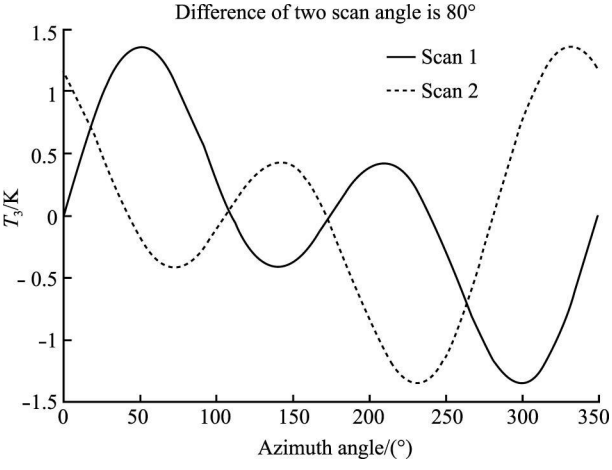


Fig. 3 $T_3$ in two different scan angles as a function of the true wind direction

The first rank solutions for each true wind direction of one scan are shown in Fig. 4 (a). The median filtering solutions for each true wind direction are shown in Fig. 4 (b). In order to isolate the effect of ambiguous solutions on the wind vector retrieval errors, the retrieval algorithm was modified to generate an additional wind vector estimated by choosing the closest solution to the true wind vector in the first rank and second rank solutions of one scan. This estimate corresponds to the closest solution to the true wind vector of one scan. These results are shown in Fig. 4 (c). An additional wind vector was estimated by choosing the closest solution to the true wind vector in the first rank solutions of two scans and second rank solution of the first scan. This estimate corresponds to the closest solution to the true wind vector of two scan. These results are shown in Fig. 4 (d).

The error of MLE solution based on only one scan is 61.69°, as indicated in Fig. 4 (a). The error of MF initialized with MLE solution is 50.36°, as indicated in Fig. 4 (b). The error of the closest solution based on only one scan is 26.82° and that based on two scans is 15.18°, as indicated in figures 4 (c) and (d). Of all the above four solutions, the closest solution based on two scans give the best result of retrieved wind direction. Since true wind direction couldn't be known in practical application of obtaining near-surface winds over the global oceans using satellites, the closest solution would not be archived.

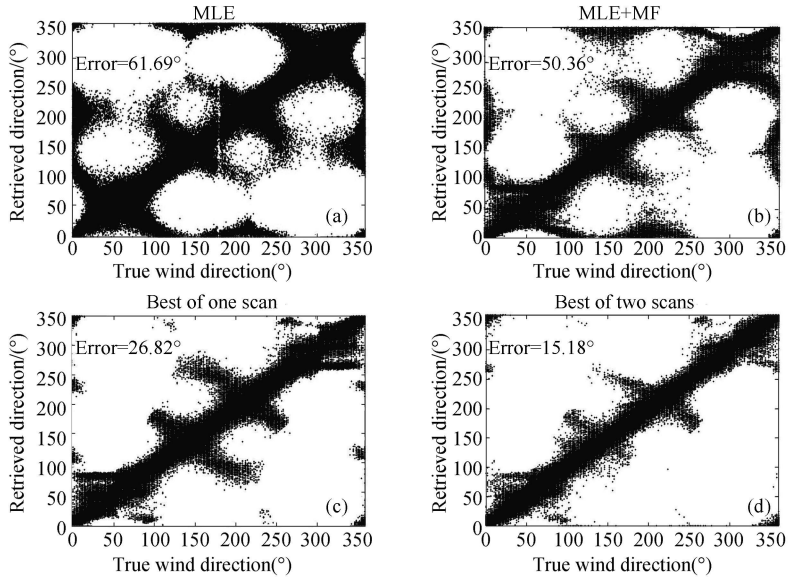


Fig. 4 Comparison of retrieved wind direction versus true value from different methods
(a) MLE; (b) MLE with median filter; (c) the Closest solution of one scan; (d) the Closest solution of two times scans

## 4 CONSIDERATION FOR PRACTICAL APPLICATION

As true wind direction couldn't be known in practical we proposed an algorithm to obtain wind direction according to first and second rank solutions of the first scan and first rank solution of the second scan, as shown in Fig. 5. In Fig. 5, $\varphi_I$ is the direction initialized for median filtering; $\varphi_{f1}$ is first rank solution of the first scan; $\varphi_{f2}$ is second rank solution of the first scan; $\varphi_{b1}$ is first rank solution of the second scan; and $a_1 = |\varphi_{f1} - \varphi_{b1}|$, $a_2 = |\varphi_{f2} - \varphi_{b1}|$, $a_3 = |\varphi_{f1} - \varphi_{f2}|$. The result of median filtering gives the final retrieved wind direction.

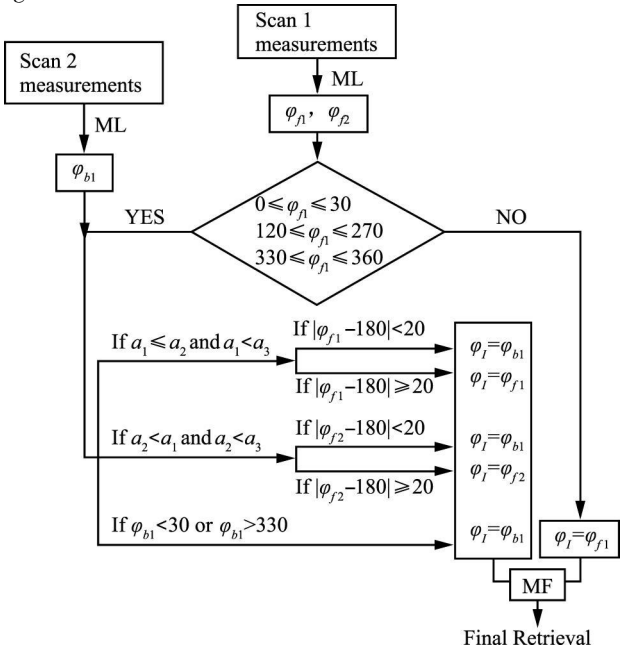


Fig. 5 Simplified flow chart of the retrieval algorithm

This algorithm gives different performances with different wind speeds and scan angles in two scans.

Fig. 6 shows that when wind speed is higher than 10m/s our algorithm performs the same as the closest solution of two times scans which is impossible to obtain actually, and much better than the first rank solution of only one scan, given that the difference of scan angles of two scan is 80°. The wind direction error in Fig. 6 is calculated all over the 360° of true wind direction. When wind speed decreases, the performance of our algorithm decreases. As wind speed $< 4$m/s, our algorithm performs almost the same as the first rank solution of only one scan. This is thought to be caused by the fact that the amplitude of the wind-direction-dependent signal decreases as wind speed decreases, and the mean wind direction errors of the first rank solutions for two scans increase as wind speed decreases.

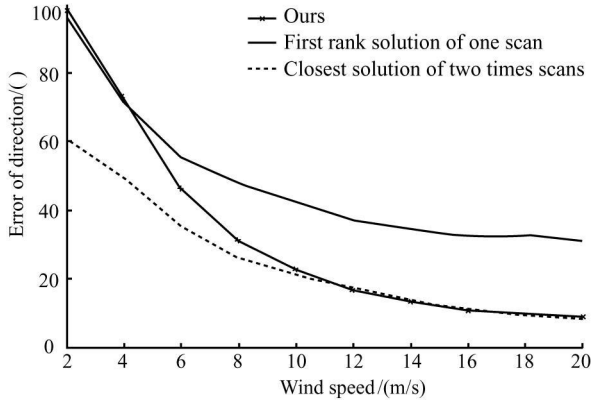


Fig. 6 Wind direction error as a function of the wind speed

Fig. 7 shows errors of wind direction versus wind speed and differences of scan angles. As indicated in Fig. 7, the performance of this new algorithm changes with the

difference of two scan angles. Meanwhile, errors of wind direction are smaller with higher wind speed.

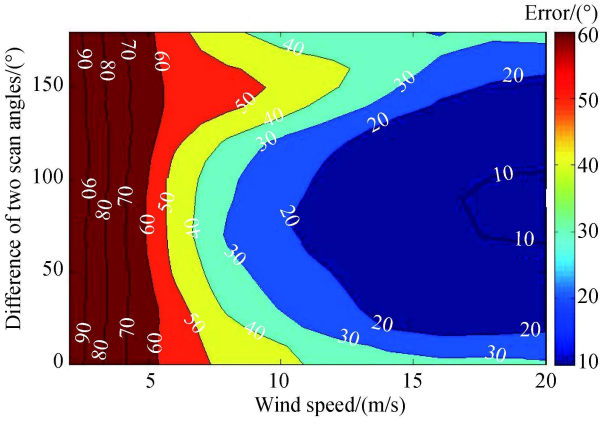


Fig. 7 Errors of wind direction versus wind speed and differences of scan angle

Fig. 8 shows differences of errors of wind direction from the new algorithm and closest solution of two times scans versus wind speed and differences of scan angles. As indicated in Fig. 8, differences of errors of wind direction from the new algorithm and closest solution of two times scans changes with the difference of two scan angles. These differences are the lowest with differences of scan angle being 90°. Meanwhile, these differences are smaller with higher wind speed.

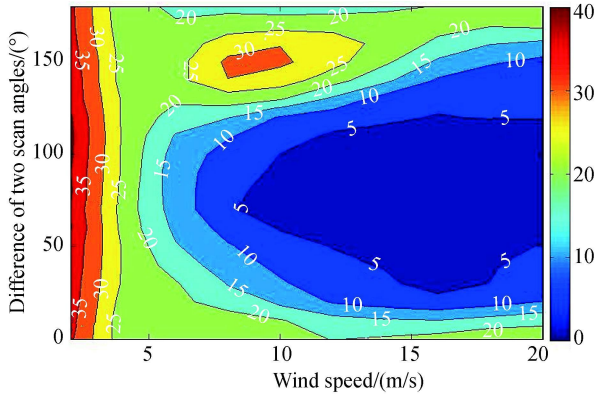


Fig. 8 Differences of errors of wind direction from the new algorithm and closest solution of two times scans versus wind speed and differences of scan angle

The relation between antenna scan azimuth angles $\varphi_1$ of forward-looking and $\varphi_2$ of backward-looking for the same ground cell is $\varphi_1 + \varphi_2 = 180°$. Suppose that $\varphi_1$ and $\varphi_2$ are measured clockwise from the forward direction of satellite, the difference of scan angles ($\alpha$) between for-look and aft-look for the same ground cell is as follows:

$$\alpha = 180 - 2 \times \varphi_1 \quad (5)$$

Based on the new algorithm developed in this paper, a method to improve calibration accuracy by creatively designing fully onboard calibrator and reasonably allocating time for calibration and observation during one scan cycle are demonstrated in the next issue of Journal of Remote Sensing. (Wang et al, 2009)

## 5 SUMMARIES

Expected errors in wind direction retrievals have been examined using sensitivity analysis techniques, Monte Carlo simulation analysis, and examination of the MLE cost function in the presence of noise. The case with errors due to upwind/downwind ambiguities was focused on in simulated retrievals. The magnitude of errors observed in retrievals from simulated data without ambiguity removal are generally much larger than in those predicted by the closest solutions to true wind direction, and a strong dependence on the true relative wind direction are observed in our study.

Since true wind direction couldn't be known in application of obtaining near-surface winds over the global oceans from satellites, the closest solution will not be archived. We proposed an algorithm to obtain wind direction according to first and second rank solutions of the first scan and first rank solution of the second scan. When wind speed is high, for example higher than 10m/s, our algorithm performs the same as the closest solution. When wind decreases, the performance of our algorithm decreases. This is thought to be caused by the fact that mean wind direction errors of the first rank solutions for two scans increase as wind speed decreases.

Considerations on practical application have been presented. The algorithm based on closest solution of two scans gives different performances of removing upwind/downwind ambiguity as the angle $\alpha$ changes. The cells near the position that along or perpendicular to spacecraft-heading vector give the largest error of retrieved wind direction. These cells can be used for cold and warm calibration, and the residual cells which give smaller direction errors can be used for wind direction remote sensing. And a new scanning geometry for conical-scan has been put forward.

Acknowledgements This study is supported by China Postdoctoral Science Foundation funded project No. 20070420070.

## REFERENCES

Adams I S, Hennon C C, Jones W L, et al. 2006. Evaluation of hurricane ocean vector winds from WindSat. IEEE Transactions on Geoscience and Remote Sensing, **44** (3): 656-667.

Bettenhausen M H, Smith C K, Bevilacqua R M, et al. 2006. A nonlinear optimization algorithm for WindSat wind vector retrievals. IEEE Transactions on Geoscience and Remote Sensing, **44** (3): 597-608.

Brown S T, Ruf C S, Lyzenga D. 2006. An emissivity-based wind vector retrieval algorithm for the WindSat polarimetric radiometer. IEEE Transactions on Geoscience and Remote Sensing, **44** (3): 611-621.

Chang P S, Li L. 1998. Ocean surface wind speed and direction retrievals from the SSM/I. IEEE Transactions on Geoscience and Remote Sensing, **36** (6): 1866-1871

Gaiser P W, Germain K M, Twarog E M, et al. 2004. The WindSat spaceborne polarimetric microwave radiometer: sensor description and early orbit performance. IEEE Transactions on Geoscience and Remote Sensing, **42** (11): 2347-2361

Germain K S, Poe G, Gaiser P. 2002. Polarimetric emission model of the sea at microwave frequencies and comparison with measurements. Progress In Electromagnetics Research, **37**: 2-32

Goodberlet M A, Swift C T, Wilkerson J C. 1990. Ocean surface wind speed measurements of the special sensor microwave/Imager (SSM/I). IEEE Transactions on Geoscience and Remote Sensing, **28** (5): 823-828

Jones W L, Cardone V J, Pierson W J, et al. 1999. NSCAT high resolution surface winds measurements in typhoon violet. Journal of Geophysical Research, **104** (C5): 11247-11260

Jones W L, Zec J. 1996. Evaluation of rain effects on NSCAT wind retrievals. The Oceans 96 Conf. Ft. Lauderdale, FL, Sept. 23-26

Laws K E, Lyzenga D R, Wiberg D M, et al. 2006. Characterization of errors in vector wind retrievals from satellite-based polarimetric microwave radiometer measurements. IEEE Transactions on Geoscience and Remote Sensing Letters, **3** (1): 45-48

Liu J Y, Wang Z Z, Yin X B, et al. 2008. Ocean wind retrieval from the brightness temperature data of the windSat microwave polarimetric radiometer. Chinese High Technology Letters, **18** (5): 519-524 (in Chinese)

Meissner T, Wentz F. 2002. An updated analysis of the wind direction signal in passive microwave brightness temperatures. IEEE Transactions on Geoscience and Remote Sensing, **40** (6): 1230-1240

Meissner T, Wentz F. 2005. Ocean retrievals for WindSat: radiative transfer model, algorithm, validation. Proceedings of IGRASS'05, Santa Rosa, July 25-29

Piepmeier J R, Gasiewski A J. 2001. High-resolution passive polarimetric microwave mapping of ocean surface wind vector fields. IEEE Transactions on Geoscience and Remote Sensing, **39** (3): 606-622

Shaffer S J, Dunbar R S, Hsiao S V, et al. 1991. A media-filter-based ambiguity removal algorithm for NSCAT. IEEE Transactions on Geoscience and Remote Sensing, **29** (1): 167-174

Smith C K, Bettenhausen M, Gaiser P W. 2006. A statistical approach to WindSat ocean surface wind vector retrieval. IEEE Transactions on Geoscience and Remote Sensing Letters, **3** (1): 164-168

Wang Z Z, Liu J Y, Yin X B, et al. 2008. Removing upwind/downwind ambiguity of ocean wind direction by polarimetric microwave radiometer-Scheme design on on-orbit calibration and scanning geometry. Journal of Remote Sensing, In press

Weissman D E, Bourassa M A, O'Brien J J, et al. 2003. Calibrating and validating the QuikSCAT/SeaWinds radar for measuring rain Rate over the ocean. IEEE Transactions on Geoscience and Remote Sensing, **41** (12): 2814-2820

Wentz F J, Meissner T, Smith D K. 2005. Assessment of the initial release of windSat wind retrievals. RSS Technical Report. America

Wentz F J. 1992. Measurement of oceanic wind vector using satellite microwave radiometers. IEEE Transactions on Geoscience and Remote Sensing, **30** (5): 960-972

Wentz F J. 1997. A Well-calibrated ocean algorithm for SSM/I. Journal of Geophysical Research, **102** (C4): 8703-8718

Yueh S H, Wilson W J, Dinardo S, et al. 2006. Polarimetric microwave wind radiometer model function and retrieval testing for WindSat. IEEE Transactions on Geoscience and Remote Sensing, **44** (3): 584-596

Yueh S H, Wilson W J, Dinardo S, et al. 1999. Polarimetric microwave brightness signatures of ocean wind directions. IEEE Transactions on Geoscience and Remote Sensing, **37** (2): 949-959

Yueh S H, Wilson W J, Dinardo S J, et al. 2006. Polarimetric microwave wind radiometer model function and retrieval testing for WindSat. IEEE Transactions on Geoscience and Remote Sensing, **44** (3): 584-596

Yueh S. 1997. Modeling of wind direction signals in polarimetric sea surfaces brightness temperatures. IEEE Transactions on Geoscience and Remote Sensing, **35** (6): 1400-1418

# 一种消除全极化微波辐射计顺/逆风向遥感模糊性的新方案

## ——算法研究

殷晓斌, 王振占, 刘璟怡, 姜景山

中国科学院空间科学与应用研究中心, 北京 100190

**摘 要**: 全极化微波辐射计可以进行海面风速和风向测量。由于地物模型函数本身的特征以及辐射计的各种测量噪声,通常会出现最后反演出的风向往往不是与真实风向最接近的情况。如果不进行全极化辐射计扫描观测单元与定标单元的优化设置,可能会出现风向反演的顺/逆风180°模糊性问题。这将大大降低全极化辐射计海面风向反演的精度。采用Monte Carlo方法研究全极化辐射计海面风向反演出现的顺/逆风向模糊性的特点和消除方案。根据模拟反演的结果,提出一种根据第一次扫描的第一、第二风向解和第二次扫描的第一风向解选择最终风向值的算法。该算法消除了顺/逆风向反演的模糊性,在一定程度上提升了全极化辐射计的性能,并为进一步设计全极化辐射计的星上实际应用方案提供了理论依据。

**关键词**: 海面风向,全极化辐射计,顺风,逆风,模糊性